CHARACTERISTICS REPRODUCIBILITY OF $(Fe,Co)(Cr,Al)_2O_4$ PIGMENTS OBTAINED BY SOLUTION COMBUSTION SYNTHESIS

J. Gilabert[1,*], M.D. Palacios[2], V. Sanz[2,3], S. Mestre[2,3]

[1]Instituto de Tecnología Cerámica. Asociación de Investigación de las Industrias Cerámicas. Castellón (Spain)

[2]Instituto Universitario de Tecnología Cerámica. Universitat Jaume I. Castellón (Spain)

[3]Departamento de Ingeniería Química. Universitat Jaume I. Castellón (Spain)

*Corresponding Author (jessica.gilabert@itc.uji.es)

1 Abstract

Synthesis reproducibility of mixed spinels $Fe_{1-\Psi}Co_{\Psi}Cr_{2-2\Psi}Al_{2\Psi}O_4$ ($0 \leq \Psi \leq 1$), obtained by Solution Combustion Synthesis using urea as fuel, has been studied. Pigments with spinel structure Fd-3m have been obtained for all the compositional range analyzed. Characteristics such as crystallinity, cell parameter, crystal size and specific surface area show a noticeable dependence with Ψ, but some of them present a low reproducibility, indicating a pronounced dependency with process conditions in each batch.

Colouring power of synthesized pigments is highly significant, so they can be directly integrated in ceramic glasses without introducing a second thermal treatment. However, the generated colour also suffers from a limited reproducibility.

Keywords: Powders: chemical preparation (A); colour (C); spinels (D); reproducibility

2 Introduction

Solution combustion synthesis (SCS) is an innovative method to synthesize ceramic pigments, which allows obtaining materials in a direct pathway, with a low particle size, using short reaction times and moderate temperatures [1].

Experimental results reported on this topic show that the traditional methodology for preparation of spinels via ceramic method involves annealing at temperatures up to 1400ºC and long soaking times [2]. During this thermal treatment, solid state reactions take place and the chromophore cations are incorporated into the newly generated host lattice. However, due to the elevated temperature reached during the process, the resulting pigment presents low specific surface area and high particle size, which is reflected in a low colouring power. For this reason, in the industrial practice a milling operation of the pigment is mandatory in order to obtain a marketable product. In addition, the ink-jet technology applied to ceramic decoration requires pigments with a particle size around 500 nm, which supposes an increase in the cost of the milling stage and a change in the milling technology. As a consequence, there is a growing demand for alternative routes for synthesizing pigments that give directly particle sizes near to the interval recommended for ink-jet machines. SCS is a method suitable to overcome some important disadvantages of ceramic pigment traditional processing because it could generate pigments as low cohesive masses formed of nanograins, easier to mill up to the submicrometer interval.

SCS method begins with a concentrated aqueous solution of precursors of the desired product (being the nitrates the most frequently used), and a suitable fuel (glycine, urea, hexamethylentetraamine, hydrazine and their derivates, etc.). The solution is heated at high rate in order to evaporate all water and, afterwards, to ignite the fuel present in the solid residue, which supplies enough energy to carry out the synthesis reaction. The reaction product is frequently obtained as a spongy mass.

SCS has been used to synthesize large number of inorganic materials, either simple oxides (α-Al_2O_3 [3], ceria [4], γ-Fe_2O_3 [5], magnetite [6], anatase [7], zirconia [8] and cobalt oxides [9]), or mixed oxides with different complexity (wollastonite [10], $CaAl_2O_4$ [11], YAG [12], doped MgO [13], $Ti_{1-x}M_xO_2$ [14], perovskites [15-17]). In addition, due to SCD high versatility to obtain complex structures, some research groups have investigated the synthesis of ceramic pigments by means of this method. Patil et al. have obtained many spinels, as $CoAl_2O_4$ [18], $Cr_xAl_{2-x}O_3$ [19], and also Zn and Ni ferrites [20] and Co, Cu and Fe chromites [21]. Afterwards, other groups have studied other mixed oxides as the ones derived from the ZnO-NiO-Fe_2O_3 [22], CoO-FeO-Cr_2O_3 [23] and ZnO-CoO-Al_2O_3 [24] systems.

Most of the spinel-type ceramic industrial pigments include more than three metals in their composition to adjust the final colour. As a consequence, it was investigated whether SCS was adequate to synthesize complex spinels. The system FeO-CoO-Cr_2O_3-Al_2O_3 was selected for the research, because it could cover a wide palette of colours, being the extreme spinels $FeCr_2O_4$ and $CoAl_2O_4$ two of the most common pigments used in the traditional ceramic sector as the Color Pigments Manufacturers Association defines [25]. On the other hand, since the pigments prepared by SCS are candidates to develop suitable inks to be used in the inkjet technology, the reproducibility of the synthesis process was analysed because it would be an

essential factor to consider in regards to a possible scaling-up of the method to an industrial level.

3 Experimental procedure

The pigments were designed as solid solutions of two spinels with high colouring power, such as brown $FeCr_2O_4$ and blue $CoAl_2O_4$. Consequently, their compositions corresponded to the formula $Fe_{1-\Psi}Co_{\Psi}Cr_{2-2\Psi}Al_{2\Psi}O_4$ ($0 \leq \Psi \leq 1$ in steps of 0.2). Solutions were prepared from their corresponding nitrates, using urea as fuel (all reactants were from Panreac Química, S.A.U. Spain), and distilled water as solvent. The addition of urea was calculated following the reaction stoichiometry in order to assure the complete combustion of the mixture (table 1).

The solution was placed in a pyrex container of 11 cm in diameter and 350 mL capacity which was introduced in a kiln preheated at 500 ºC (BLF 1800, Carbolite Furnaces Ltd, UK). After 20 minutes of soaking time, the kiln was turned off and allowed to cool the sample. Three replicas were obtained for every composition.

Every synthesized pigment was wet milled in water in a ball mill, using agate jars (Pulverisette 5, Fritsch GmbH, Germany). The evolution of the crystalline phases present, the crystal size and the cell parameters as a function of composition were monitored by XRD (Theta-Theta D8 Advance, Bruker, Germany), with CuKα radiation (λ = 1.54183 Å). The generator settings were 45 kV and 40 mA. The XRD data were collected in a 2θ of 5–90º with a step width of 0.015º and a counting time of 1.2 s/step by means of a VÅNTEC-1 detector. The collected data were used in a Rietveld refinement. The 4.2 version of the Rietveld analysis program DIFFRACplus TOPAS was used, assuming a pseudo-Voight function to describe peak shapes. The refinement protocol included the background, the scale factors and the global-

instrument, lattice, profile and texture parameters. The specific surface area was determined according to the BET method using the adsorption isotherm and nitrogen gas as adsorbent (Tristar 3000, Micromeritics, USA). The microstructure of the samples was characterized by FEG-SEM (QUANTA 200F, FEI Co, USA). Chemical composition was determined by an energy-dispersive X-ray microanalysis instrument (Genesis 7000 SUTW, EDAX, USA) coupled to the FEG-SEM. Moreover, oxidation state of the elements was studied by means of X-ray photoelectron spectroscopy (XPS) using a Specs SAGE 150 instrument. In order to identify all the elements present, the range of binding energies was analysed between 1100 eV and -5 eV. The analyses were performed using non-monochrome AlKα irradiation (1486.6 eV) at 20 mA and 13 kV, a constant energy pass of 75 eV for overall analysis, 30 eV for analysis in the specific binding energy ranges of each element, and a measurement area of 1x1 mm^2. The pressure in the analysis chamber was $8 \cdot 10^{-9}$ hPa. The energy corrections of the spectra were performed considering a reference value of C 1s owing to the organic matter at 284.8 eV.

Colour development was evaluated by introducing every pigment into a transparent fast-firing wall tile glaze (chemical composition 0.5% Na_2O 4.0 % K_2O, 15.3% CaO, 0.9 MgO, 9.0% ZnO, 7.4% Al_2O_3, 3.0% B_2O_3, 59.5% SiO_2). A 2/98 wt% slip was applied over a fired wall tile, and afterwards, fired together in an electric laboratory kiln according to a thermal cycle of single-fired floor tiles (maximum temperature 1100 ºC and 6 min of soaking time at this temperature). The spectrophotometric curve and CIELab chromatic coordinates of the glazed surfaces were determined using CIE Illuminant D_{65} and CIE 10º standard observer (Color Eye 7000A, X-Rite Inc, USA).

4 Results and discussion

Synthesized pigments covered a wide colour palette, from dark brown to dark green, passing through different grey intensities and even black. Colour gradients were absent in the as-obtained mass, which indicates a good chemical homogeneity in the pigments. Regarding their consistence, an important evolution in the final product was observed, due to the fact that when $\Psi = 0.0$ a very spongy mass was obtained, but while as Ψ was increasing, the mass was progressively reducing their porosity, indicating a gradual change in the reaction mechanism. The spongy consistence of the pigments can be justified because of the high volume of gases generated during the combustion process. However, it has also been described that in the case of urea the volume of gases is not high enough to dissipate rapidly the heat of reaction, which favours the product sintering [21], which could be the cause of the change in the consistence.

4.1 Chemical composition

EDX analysis was used to evaluate the chemical homogeneity of the pigments. Figure 1 shows the molar percentage of the five elements as a function of Ψ. The results confirmed that pigment synthesis have been developed in a very effective way. The homogeneity in the distribution of metals was good, since experimental values follow the theoretical path. That behaviour means the reaction takes place following stoichiometric proportions, so the energy generated by the combustion of urea is far enough to synthesize the desired spinel, always talking from a chemical homogeneity point of view.

With respect to oxygen, pigments with higher percentages of Fe and Cr showed an O content slightly superior to the theoretical value, which could be associated to changes in the state of oxidation of iron. In figure 2 can be observed that the peak deconvolution of the XPS spectrum obtained to measure the electronic state of iron in the $FeCr_2O_4$ spinel (Ψ=0) clearly indicates the presence of both Fe^{2+} and Fe^{3+} cations in the structure. By contrast, pigments richer in Al and Co presented an oxygen content more similar to the theoretical one.

According to the reproducibility of data, the pigment composition was relatively stable, independently of the Ψ-value considered. However, it has been observed a higher deviation from the stochiometric composition when $\Psi \geq 0.8$, phenomenon that could reveal some difficulties to obtain a completely homogeneous composition for the $CoAl_2O_4$ spinel in the short time of reaction.

The results demonstrate the effectiveness of SCS reaction to develop a homogeneous product which includes more than three metals.

4.2 Crystalline structures

XRD analysis showed that all samples possessed a spinel structure, face centred cubic crystal phase (space group Fd-3m) whose main intensity peaks ranged between the reflections of pure $FeCr_2O_4$ and $CoAl_2O_4$ spinels. No signals of free oxides not integrated in the structure were detected, indicating a perfect development of spinel-type structure. However, composition of initial mixture exerted a pronounced effect on cell parameters and crystal size of spinels.

The evolution of the main X-ray reflection pattern of the spinel (I_{100}), as function of Ψ–value, shows important events regarding the formation of the spinel structure (Fig. 3). Contrary to what might be expected, pure spinels are not the ones that

present the highest crystallinity. In fact, the intensity of the main peak increases as reduced proportions of Co and Al cations are integrated in the $FeCr_2O_4$ spinel. Mixtures with Ψ values between 0.2 and 0.4 promote a considerable improvement of the pigment crystallinity, since their I_{100} is higher than in the rest of the cases. However, if Ψ is further increased, the pigments show a progressive decrease in their crystallinity and, as a consequence, the diffraction peak becomes practically an amorphous hallo for Ψ=1. In other words, when the composition of the solution is designed to obtain the $CoAl_2O_4$ (Ψ=1), the product has a low crystallinity because this spinel is highly difficult to crystallize in SCS conditions. Experimental behaviour observed in the XRD patterns is consistent with the evolution of crystal size (Fig. 4) determined by Rietveld adjustment since a maximum in crystal size was observed when the spinel crystallinity was the highest (Ψ = 0.2). The smallest crystals were measured in the cobalt aluminate pigments, and the biggest ones in the cobalt-rich chromite structures, but the descending progress was more pronounced for $\Psi \geq 0.6$, corroborating the negative effect of aluminium and cobalt ions on the crystallization of the spinel.

As some authors have studied [1], SCS is adequate to prepare non-transition metal aluminates that are totally crystalline and spongy; but there are some disadvantages when transition metal aluminates like $CoAl_2O_4$ are synthesized because they are thermally unstable at that temperature. Referring to its equilibrium phase diagram [26], $CoAl_2O_4$ is absolutely stable at temperatures achieved during SCS process (~ 1500ºC), as long as the mixture follows the correct stoichiometry because sample temperature is far below its melting point (1980ºC). Thus taking into account both references, it could be thought that one of the reasons for the lack of crystallinity for $CoAl_2O_4$ spinel is the fast kinetics of the reaction. In fact, the process is too fast to

allow the cation reorganisation to obtain a highly crystalline spinel because during the drying process to obtain the gel, there could be a segregation between the different salts. This phenomenon only happens in the case of Co and Al precursors but not in the case of Fe and Cr ones.

Regarding crystallinity of the mixtures, the effect of exchanging Fe^{2+} ion by Co^{2+} in the iron-chromite spinel was studied in previous works [23], observing an improvement in the pigment crystallinity as the Co content increased. Therefore, taking into account the isolated effect of the Co element, what it seems to happen is that Co helps to improve crystallinity of chromite remaining unalterable spinel structure. However, Al^{3+} cation acts in a different way, possibly because it has lower ionic radii than Cr^{3+}, and this fact could difficult crystallization under SCS conditions.

The general trend of lattice parameters of the cell was consistent with the lower ionic radius of the Al^{3+} (0.39 Å) with respect to the Cr^{3+} (0.62 Å) in octaedric coordination, since the ionic radii of the divalent ions in tetraedric coordination are similar (0.65 and 0.61 Å for Co^{2+} and Fe^{2+}, respectively). The lower the ion size is, the shorter the distance between ions becomes and, as a consequence, the lattice parameter decreases since dimensions of the spinel cell are reduced [27]. Figure 5 shows the evolution of the cell parameter obtained by Rietveld method as a function of Ψ. As it can be observed, lattice parameter ranges from pure Fe-chromite (reported value 8.26 Å [28]) to Co-aluminate (8.06 Å [29]). The evolution was less linear than expected according to the Vegard's law, because a positive deviation from the estimated values was clearly observed. Experimental data decrease at an approximate constant rate from $\Psi = 0.0$ to $\Psi = 0.6$, which could mean that the pigment structure remains relatively similar to $FeCr_2O_4$. But at $\Psi \geq 0.6$ appears an

inflexion point from which lattice parameter undergoes a more pronounced downward trend, and the lattice parameter resembles to $CoAl_2O_4$ spinel. This behaviour has been previously observed in other spinel systems by Shou-Yong et al. [30] and Nlebedim et al. [31], however, no generally accepted explanation has been proposed yet for this phenomenon.

Apart from the general trend obtained for crystallinity and crystal size, it has been observed certain variability of these properties in some compositions. The reproducibility of the method indicates that the fast reaction kinetics of SCS difficults to reach the equilibrium structure of the spinels. This effect is especially appreciable when the highest grades of crystallinity are expected ($0.2 \leq \Psi \leq 0.4$). Unless all process conditions in the synthesis are maintained under strict control, pigment crystallinity could show wide variations because of their fast kinetics.

4.3 Morphology and grain size

Specific surface area was selected as a parameter directly related to pigment microstructure, allowing the study of pigment morphology related to the change in the composition of spinel. Only for the composition with $\Psi = 0.2$, which was the one that presented more variability in XRD analysis, the measurements were carried out in the three replicas, and thus it was possible to evaluate the variability of this parameter.

Specific surface area was maintained practically stable in the range from $\Psi = 0.0$ to $\Psi = 0.6$, since it oscillated inside a defined band of 26 ± 8 $m^2 \cdot g^{-1}$. However, it was observed a change in the trend for higher values of Ψ. This is because the specific surface area increased considerably from this point, until achieving values around 200 $m^2 \cdot g^{-1}$ for the pigment corresponding to $CoAl_2O_4$ spinel. This fact pointed out an

important modification in the microstructure of the pigment. In this case, the SEM images allowed understanding the results of a specific surface area (Fig. 6). Pigments corresponding to Ψ values from 0.0 to 0.6 showed a microstructure composed by well-sintered rounded grains. These were forming agglomerates with low porosity and practically smooth surfaces, which correlates with a moderate specific surface area. However, the grain size was not homogeneous, presenting a minimum in Ψ=0.2. Pigment with Ψ=0.8 also maintained rounded grains, but the sintering grade was notably inferior, thus the agglomerates were rougher. This was totally coherent with the observed increase in the specific surface area. The microstructure changed completely for the pigment richest in cobalt (Ψ = 1.0). In fact, its morphology consisted of laminar-shaped grains with a high diameter (up to 150 nm) and a reduced thickness, being less sintered and forming porous agglomerates. All this features promoted the sharp increase in specific surface area for Ψ = 1.0 sample [32].

In addition, there is a relation between S_e and crystal size (Fig. 7), the lowest values of crystal size corresponded to the highest values of specific surface area due to the generation of intergrain porosity when the laminar-shaped grains of the Co-rich pigment are formed. On the other hand, however, high crystal sizes developed round-shaped grains with no intergrain porosity for Fe-rich chromites.

4.4 Determination of colouring power

The incorporation of the pigment samples into a transparent glaze generated intense coloured surfaces in all cases. This confirmed that all synthesized spinels behave as ceramic pigments, despite their particles were formed by nanosized grains.

The colour palette covers from reddish brown (Ψ = 0) to intense blue (Ψ = 1), through relatively pure but little saturated blacks. It was observed in the glaze

reflectance curves (Fig. 8) that as Ψ increases, the characteristic absorption band of Fe^{2+} in tetrahedral position (occurring between 570 and 700 nm) was progressively soften. However, the characteristic reflexion of Co at 410 nm only appeared for pigment with Ψ = 1 [24]. Regarding the rest of reflexion curves, their main characteristic was the reflexion queue getting into the infrared range.

The CIELab coordinates exhibited strong correlations with the theoretical spinel composition, but with quite different trends (Fig. 9). It should be pointed out the high variability detected in the colouring power of the different replicas, which could be the consequence of the limited reproducibility observed in the XRD results.

L* showed the most complex evolution, but within the narrowest range of variation. Luminosity presented a strong minimum around Ψ = 0.8, with a variation range of about 18 units and without any symmetry regarding composition (Fig. 9a). On the other hand, L* coordinate presented a significant variability, since the mean variation range between the highest and the lowest value for every Ψ reached 2.3 units (σ-parameter). As it was deduced in previous works of Mestre et al., such marked changes in colour brightness generated by some spinels are due in part to their lower crystallinity. This would facilitate the attack by the molten glaze generated during firing [23]. a* coordinate also showed a significant minimum (Fig. 9a), with a variation range similar to L*. The variability of a* coordinate was the lowest, since σ-parameter reached 0.7 units. By contrast, b* coordinate presented a behaviour completely different, because it showed a diminishing trend without critical points and the maximum variation range (practically 50 points, fig. 9b). b* coordinate progress exhibited two different segments, but both practically linear: The first one, $0 \leq \Psi \leq 0.8$, presented a moderate slope, while the second one showed a more

pronounced descending. The variability of this coordinate was intermediate between the other two ones, since σ-parameter was 1.5 units.

Some visual similarities between crystallographic parameter behaviour and the chromatic coordinates were observed, but not with the crystal size. It is possibly because the pigments are integrated in the vitreous matrix as big-size agglomerates and not as individual crystals. Regarding cell parameters, some good correlations were identified due to the fact that cell parameters are directly influenced by composition. Luminosity (L*) and a* coordinate showed well-defined parabolic correlation with cell parameter (Fig. 10a). Nevertheless, it has to be pointed out that the synthesizing of pigments with the same cell parameter not assures the development of the same colour. This fact indicated that colouring power also depend on other non-identified factors. Regarding b* coordinate, figure 10b shows that this parameter presents a practically linear relation with cell parameter. This result correlates with the fact that the major content in cobalt and aluminium reduces the cell parameter and the generated colour tend to be more bluish.

5 Conclusions

Solution combustion synthesis has been validated as a suitable method to synthesize ceramic pigments designed as solid solutions between two spinels with a composition $Fe_{1-\Psi}Co_{\Psi}(Cr_{2-2\Psi}, Al_{2\Psi})O_4$ (being $0 \leq \Psi \leq 1$) using urea as fuel. The process is very fast and chemically homogeneous pigments are obtained, with a spongy aspect that makes them easy to disintegrate. The composition of the raw material mixture has a significant effect on the spinel cell parameter, crystallinity, crystal size and grain size. The best crystallized spinels are obtained when a slight proportion of cobalt and aluminium is incorporated to the spinel structure of Fe-

chromite ($0.2 \leq \Psi \leq 0.4$). A further increase in Ψ reduces considerably the crystallinity of the structure till obtaining nearly an amorphous product due to the small size of crystals formed. SCS pigment properties show an important dependency with process parameters because the higher crystallinity, the wider variability they present. Cell parameter is less influenced by the process because it depends basically on composition. The effect of the composition is also observed in the microstructure of particles, consisting of sintered nanosized grains. By increasing the cobalt and aluminium content in the structure, pigment grains reorganize their geometry from a sintered round-shaped nanosized particles to a completely different structure based on laminar-shaped agglomerates with higher size. All spinels exhibit a high colouring power in a transparent glaze without any additional thermal treatment, covering a fairly broad colour palette.

Acknowledgements

The authors thank Universitat Jaume I for their support in the development of this research (Project Nr. P11B2015-04).

Bibliography

[1] K.C. Patil, M.S. Hedge, T. Rattan, S.T. Aruna, Chemistry of nanocrystalline oxide materials: Combustion synthesis, properties and applications, World Scientific Publishing, Singapore, 2008.

[2] M. Llusar, A. Forés, J.A. Badenes, J. Calbo, M.A. Tena, G. Monrós, Colour analysis of some cobalt-based blue pigments, J. Eur. Ceram. Soc. 21 (2001) 1121–1130. doi:10.1016/S0955-2219(00)00295-8

[3] J.J. Kingsley, K.C. Patil, A novel combustion process for the synthesis of fine particle α-alumina and related oxide materials, Mater. Lett. 6 (1988) 427-432. doi:10.1016/0167-577X(88)90045-6

[4] M. A. Sekar, S. S. Manohar, K.C. Patil, Combustion synthesis of fine particle ceria, J. Mater. Sci. Lett. 9 (1990) 1205-1206. doi:10.1007/BF00721893

[5] K. Suresh, K.C. Patil, A combustion process for the instant synthesis of α-Fe_2O_3, J. Mat. Sci. Lett. 12 (1992) 572-574. doi:10.1007/BF00278328

[6] R. Ianoş, A. Tăculescu, C. Păcurariu, I. Lazău, Solution combustion synthesis and characterization of magnetite, Fe_3O_4, nanopowders, J. Am. Ceram. Soc. 95 (2012) 2236-2240. doi: 10.1111/j.1551-2916.2012.05159.x

[7] S.T. Aruna, K.C. Patil, Synthesis and properties of nanosized titania, J. Mater. Synth. Proces. 4 (1996) 175-176.

[8] N. Arul Dhas, K.C. Patil, Combustion synthesis and properties of tetragonal, monoclinic and partially and fully stabilized zirconia powders, Int. J. Self-Propagating High-Temp. Synth. 1(4) (1992) 576-589.

[9] W. Wen, J.M. Wu, J.P. Tu, A novel solution combustion synthesis of cobalt oxide nanoparticles as negative-electrode materials for lithium ion batteries, J. Alloys Compd. 513 (2012) 592– 596. doi:10.1016/j.jallcom.2011.11.019

[10] R.P. Sreekanth Chankrandhar, B.M. Nagabhushana, G.T. Chandrappa, K.P. Ramesh, J.L. Rao, Solution combustion derived nanocrystalline macroporous wollastonite ceramics, Mater. Chem. Phys. 95(2006) 169-175. doi:10.1016/j.matchemphys.2005.06.002

[11] M.A. Rodríguez, C.L. Aguilar, M.A. Aghayan, Solution combustion synthesis and sintering behaviour of $CaAl_2O_4$, Ceram. Int. 38 (2012) 395-399. doi:10.1016/j.ceramint.2011.07.020

[12] K. Laishram, , R. Mann, N. Malhan, Single step synthesis of yttrium aluminum garnet ($Y_3Al_5O_{12}$) nanopowders by mixed fuel solution combustion approach, Ceram. Int. 37 (2011) 3743-3746. doi:10.1016/j.ceramint.2011.05.052

[13] V.R. Orante-Barrón, L.C. Oliveira, E.D. Kelly, J.B. Milliken, G. Denis, L.G. Jacobsohn, J. Puckette, E.G. Yukihara, Luminescence properties of MgO produced by solution combustion synthesis and doped with lanthanides and Li, J. Lumin. 131 (2011) 1058-1065. doi:10.1016/j.jlumin.2011.01.022

[14] K. Nagaveni, M.S. Hedge, G. Madras, Structure and photocatalytic activity of $Ti_{1-x}M_xO_{2-\delta}$ (M = W, V, Ce, Zr, Fe and Cu) synthesized by solution combustion method, J. Phys. Chem. B. 108 (2004) 20204-20212. doi: 10.1021/jp047917v

[15] B.M. Nagabhushana, R.P. Sreekanth Chankrandhar, K.P. Ramesh, C. Shivakumara, G.T. Chandrappa, Combustion synthesis, characterization and metal-insulator transition studies of nanocrystalline $La_{1-x}Ca_xMnO_3$ ($0 \leq X \leq 0.5$), Mater. Chem. Phys. 102 (2007) 47-52. doi:10.1016/j.matchemphys.2006.11.002

[16] M.A. Raza, I.Z. Rahman, S. Beloshapkin, Synthesis of nanoparticles of $La_{0.75}Sr_{0.25}Cr_{0.5}Mn_{0.5}O_{3-\delta}$ (LSCM) perovskite by solution combustion method for solid oxide fuel cell application, J. Alloy Compd. 485 (2009) 593–597. doi: 10.4236/njgc.2011.12010

[17] T. Striker, J.A. Ruud, Effect of Fuel choice on the aqueous combustion synthesis of lanthanum ferrite and lanthanum manganite, J. Am. Ceram. Soc. 93 (2010) 2622-2629. doi: 10.1111/j.1551-2916.2010.03799.x

[18] T. Mimani, S. Ghosh, Combustion synthesis of cobalt pigments: blue and pink, Curr. Sci. India 78 (2000) 892-896.

[19] J.J. Kingsley, N. Manickam, K.C. Patil, Combustion synthesis and properties of fine particle fluorescente aluminous oxides, Bull. Mater. Sci. 13 (1990) 179-189. doi: 10.1007/BF02744944

[20] K. Suresh, N.R.S. Kumar, K.C. Patil, A novel combustion synthesis of spinel ferrites, orthoferrites and garnets, Adv. Mater. 3 (1991) 148-150. doi: 10.1002/adma.19910030306

[21] S.S. Manoharan, K.C. Patil, Combustion synthesis of metal chromite powders, J. Am. Ceram. Soc. 75 (1992) 1012-15. doi: 10.1111/j.1151-2916.1992.tb04177.x

[22] A.C.F.M. Costa, A.M.D. Leite, H.S. Ferreira, R.H.G.A. Kiminami, S. Cava, L. Gama, Brown pigment of the nanopowder spinel ferrite prepared by combustion reaction, J. Eur. Ceram. Soc. 28 (2008) 2033-2037. doi:10.1016/j.jeurceramsoc.2007.12.039

[23] S. Mestre, M.D. Palacios, P. Agut, Solution combustion synthesis of (Co,Fe)Cr_2O_4 pigments, J. Eur. Ceram. Soc. 32 (9) (2012) 1995–1999. doi:10.1016/j.jeurceramsoc.2011.11.044

[24] R. Ianoş, R. Lazău, P. Barvinschi, Synthesis of $Mg_{1-x}Co_xAl_2O_4$ blue pigments via combustion route, Adv. Powder Technol. 22 (2011) 396-400. doi:10.1016/j.apt.2010.06.006

[25] Color Pigments Manufacturers Association, Classification and chemical descriptions of the complex inorganic color pigments, fourth ed., Alexandria (VA), 2013.

[26] E.M. Levin, H.F. McMurdie, (Eds.) Phase diagrams for ceramists, vol. III Westerville: American Ceramic Society, 1975.

[27] D.R. Lide (Ed), CRC handbook of chemistry and physics, 74th ed, CRC Press, Boca Raton, 1993.

[28] A. Kyono, S.A. Gramsch, T. Yamanaka, D. Ikuta, M. Ahart, B.O. Mysen, H. Mao, R.J. Hemley, The Influence of the Jahn-Teller effect at Fe^{2+} on the structure of chromite at high pressure, Phys. Chem. Miner. 39 (2012) 131– 141. doi: 10.1007/s00269-011-0468-6

[29] R. Griessbach, P.D. Reinhardt, Untersuchungen über Erscheinungen und Veränderungen an Kobaltoxydkontakten, Z. Anorg. Allg. Chem. 281 (1955) 241-261. doi: 10.1002/zaac.19552810503

[30] J. Shou-Yong, L.Z. Jin, L. Yong, Investigation on lattice constants of Mg-Al spinels, J. Mat. Sci, Lett. 19 (2000) 225-227. doi: 10.1023/A:1006710808718

[31] I.C. Nlebedim, J.E. Snyder, A.J. Moses and D.C. Jiles, Effect of deviation from stoichiometric composition on structural and magnetic properties of cobalt ferrite,

$Co_xFe_{3x}O_4$ (x=0.2 to 1.0), J. Appl. Phys. 111 (2012) 07D704. doi: 10.1063/1.3670982

[32] M.P. Gómez-Tena, J. Gilabert, J. Toledo, E. Zumaquero, C. Machí, Relationship between the specific surface area parameters determined using different analytical techniques, Qualicer 2014: XIII World congress on ceramic tiles. Castellón: Cámara Oficial de Comercio, Industria y Navegación, 2014.

Table 1 Composition of each synthesized spinel (0<Ψ<1 in steps of 0.2)

Ref.	**Ψ**	**Urea (g)**	**$Cr(NO_3)_3 \cdot 9H_2O$ (g)**	**$Fe(NO_3)_3 \cdot 9H_2O$ (g)**	**$Co(NO_3)_2 6H_2O$ (g)**	**$Al(NO_3)_3 9H_2O$ (g)**	**H_2O (mL)**
A1	0.0	13.51	24.01	12.12	0.00	0.00	25
A2	0.2	13.21	19.21	9.70	1.75	4.50	25
A3	0.4	12.87	14.41	7.27	3.49	9.00	25
A4	0.6	12.61	9.60	4.85	5.24	13.50	25
A5	0.8	12.31	4.80	2.42	6.98	18.01	25
A6	1.0	12.01	0.00	0.00	8.73	22.51	25

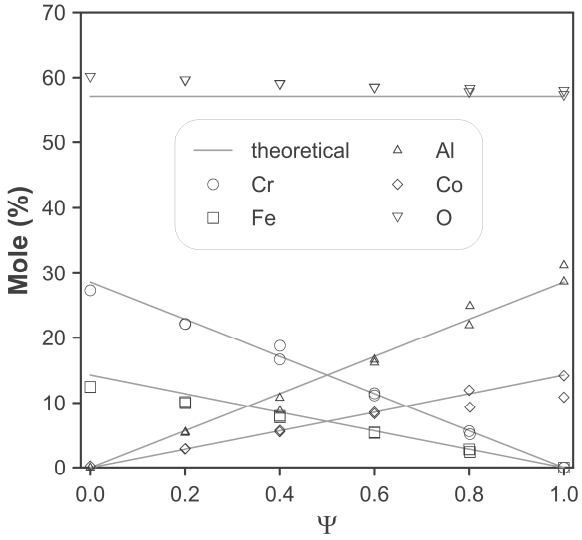

Figure 1 Comparison of theoretical stoichiometric composition (solid lines) with EDX data of pigments obtained by SCS (points)

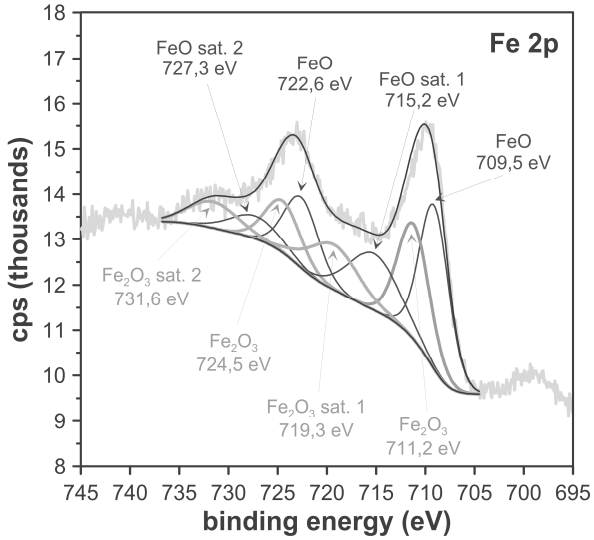

Figure 2 XPS spectrum obtained to study the electronic state of iron in the $FeCr_2O_4$ spinel (Ψ=0)

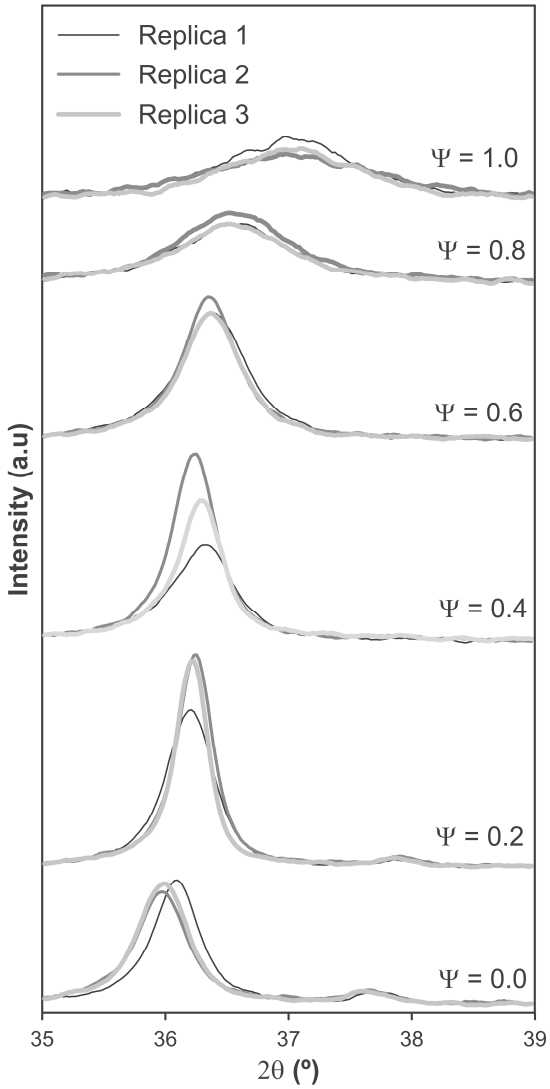

Figure 3 Evolution of the XRD's main reflection (I_{100}) of the pigments in function of Ψ and the number of replica.

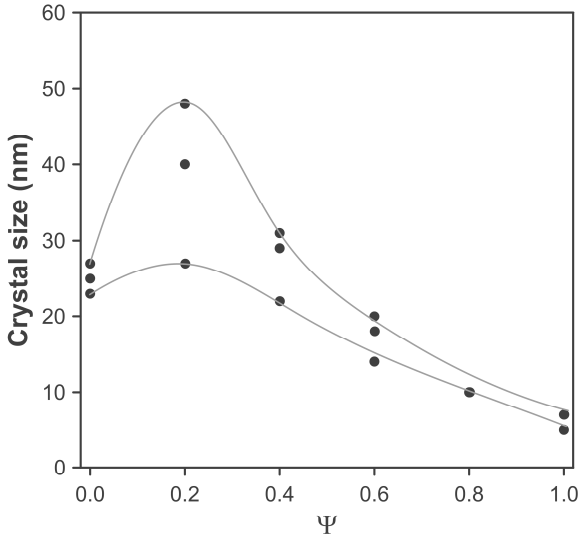

Figure 4 Evolution of crystal size depending on parameter Ψ

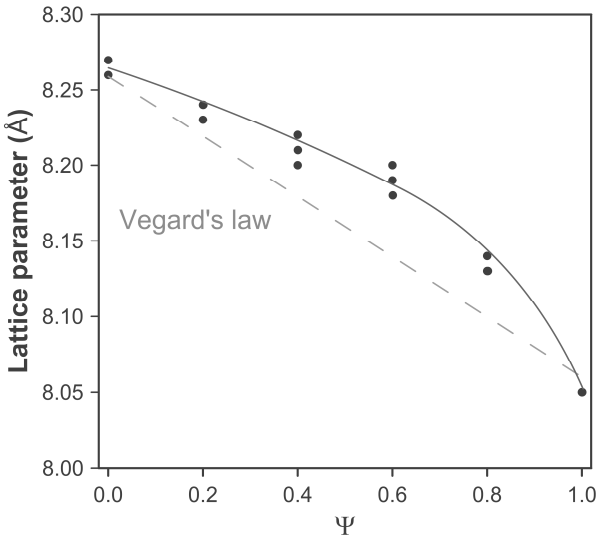

Figure 5 Comparison of cell parameters of the spinel with the prediction of Vegard's law, based on the ICCD data from the spinels $FeCr_2O4$ (Ψ = 0) and $CoAl_2O_4$ (Ψ = 1).

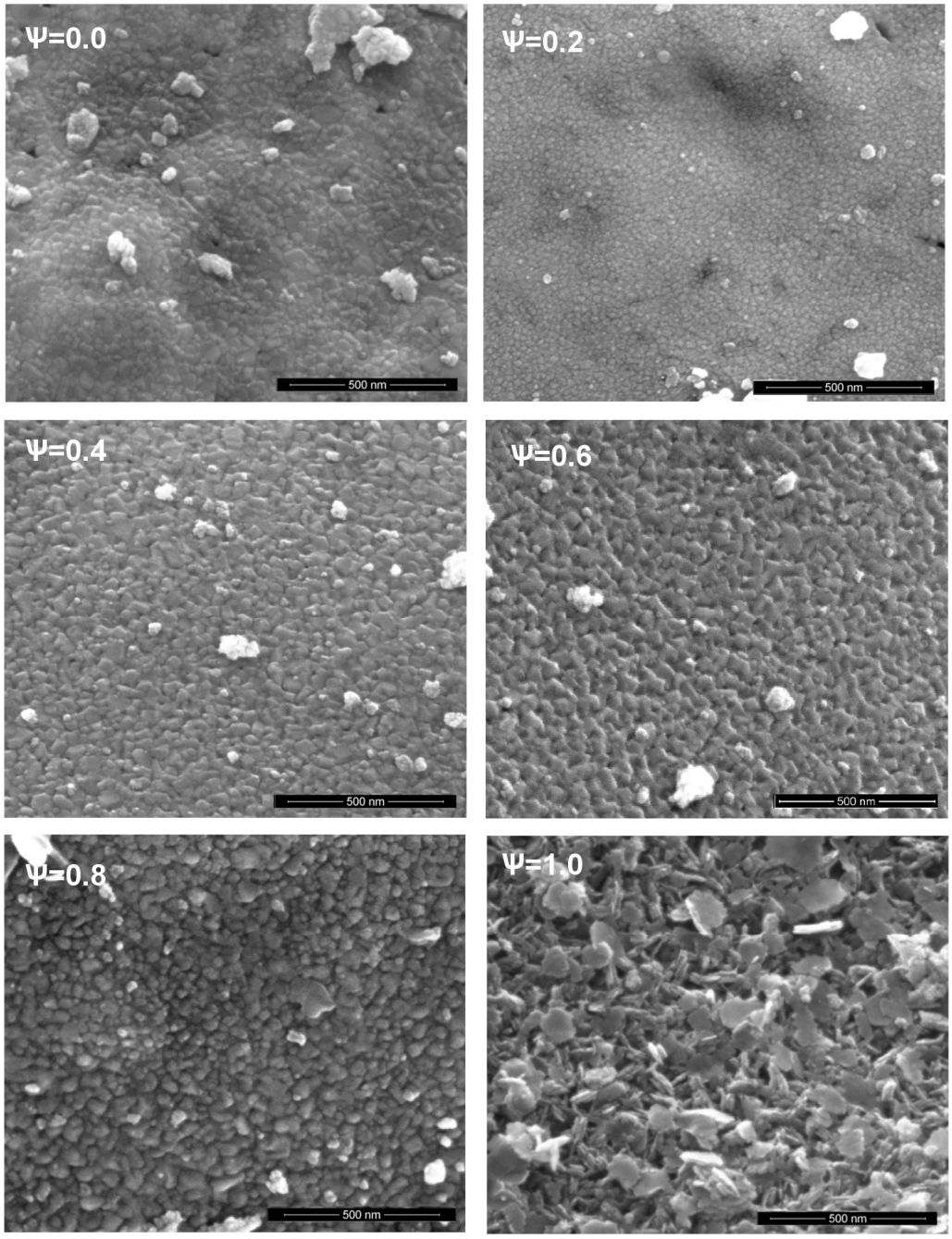

Figure 6 Micrographies obtained by SEM of synthesized pigments

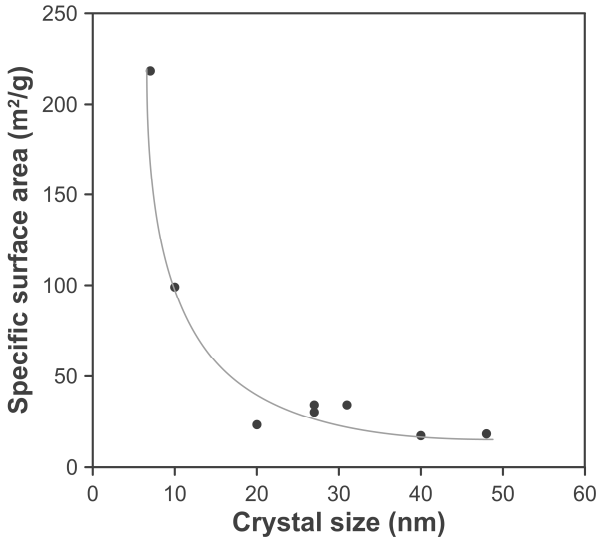

Figure 7 Evolution of specific surface area as a function of crystal size

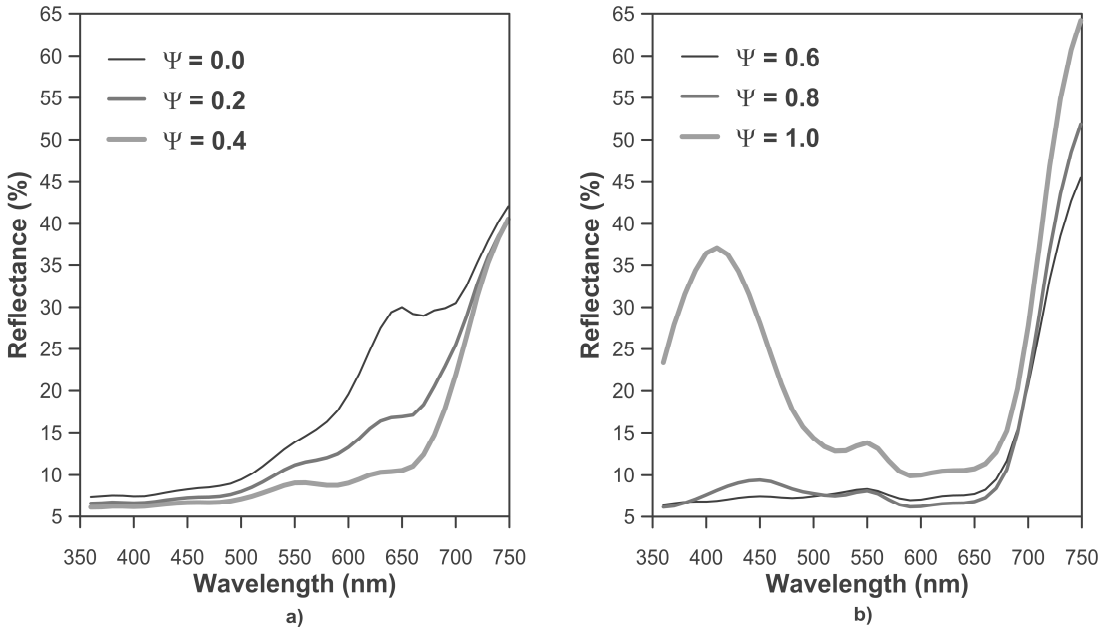

Figure 8 Reflectance curves of the glazes that contain the synthesized pigments

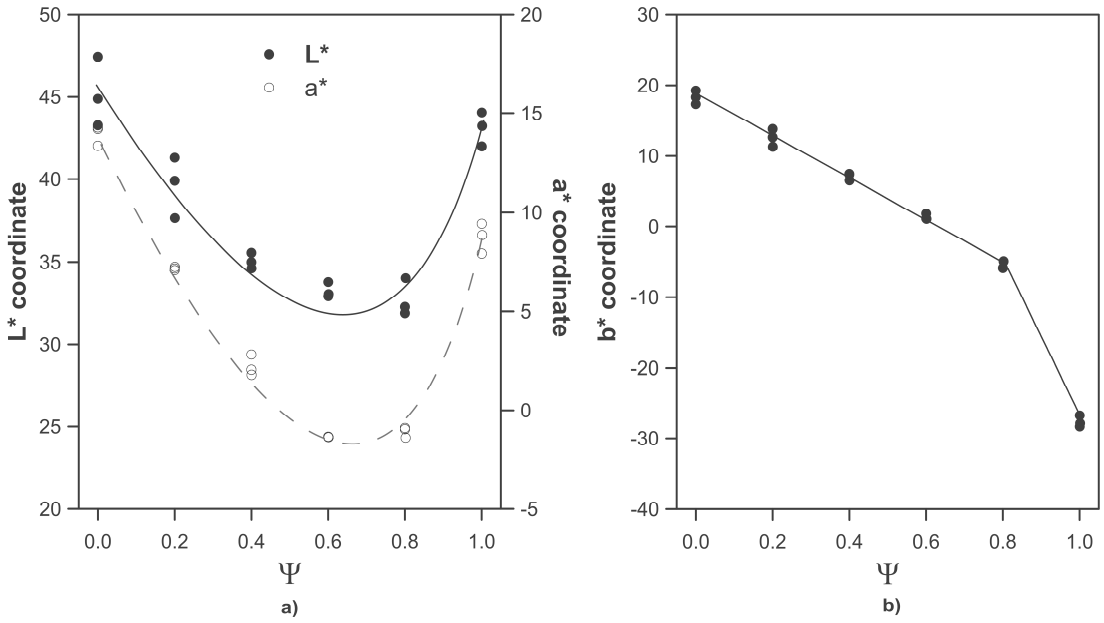

Figure 9 Evolution of chromatic coordinates of glaze as function of the composition of the incorporated pigment: a) L* and a* coordinates and b) b* coordinate

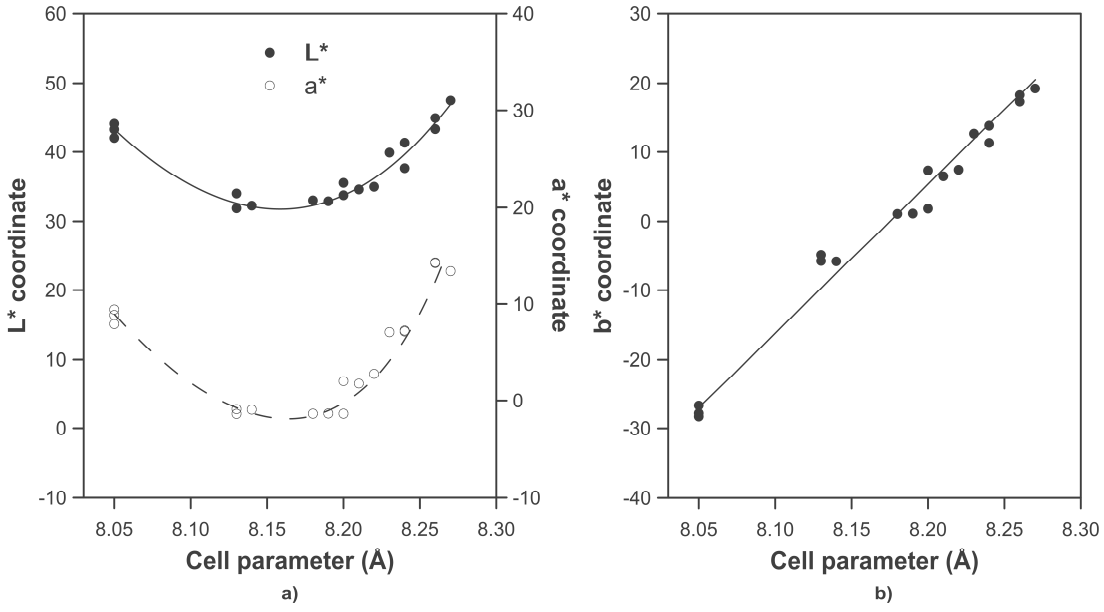

Figure 10 Evolution of chromatic coordinates of glaze as function of the incorporated pigment cell parameter: a) L* and a* coordinates, b) b* coordinate